PHYSICAL REVIEW B VOLUME 15, NUMBER 12 15 JUNE 1977

Charge-density waves in the $2H$-$TaSe_2$ family: Action on the Fermi surface

J. A. Wilson
Bell Laboratories, Murray Hill, New Jersey 07974
(Received 25 October 1976)

Recent de Haas–van Alphen measurements on $2H$-$TaSe_2$ in the $3a_0$ commensurate phase have, through their analysis, promoted a reexamination of the charge-density waves and periodic structural distortion developed in the $2H$ family of transition-metal layer dischalcogenides.

I. CHARACTERISTICS OF THE CHARGE-DENSITY WAVE (CDW) AND PERIODIC STRUCTURAL DISTORTION (PSD) IN $2H$-$TaSe_2$

Our early work[1] on the CDW's occurring in the various d^1 metallic-layer dichalcogenides concentrated, for several reasons, on the octahedrally coordinated $1T$ polytype rather than upon the trigonal prismatic ones ($2H$, $3R$, $4Hc$). First, the effects in $1T$ were much stronger and therefore more likely to be linked to a specific cause. Second, the $1T$ Fermi surface was single sheeted, and did not, furthermore, possess highly sensitive features, such as the ΓK saddle point or the ΓA dish present in the $2H$ case. Third, the $2H$ polytype was not readily amenable to cation substitutional doping, as would allow for controlled variation of the Fermi-surface (FS) dimensions.

Before proceeding I would like to draw attention to more recent data elaborating the above points. For $2H$-$TaSe_2$ the maximum cation shifts in the CDW-coupled PSD, from neutron-diffraction studies[2] turn out to be approximately 0.1 Å. On the other hand, the cation displacements in $1T$-$TaSe_2$ have been determined in recent x-ray work[3] to range up to 0.25 Å (or ~7% of a_0). Correspondingly, photoemission[4] and Mössbauer[5] measurements reveal that the amplitude of the CDW itself in the $1T$ Ta materials is such as to virtually withdraw the d^1 electron from the super-cell-cornering Ta atoms (1 in 13 of the total). By contrast NMR in $2H$-$NbSe_2$ indicates a charge redistribution amplitude of only 5% to 10%.[6] A similar contrast appears in lock-in to the commensurate states ($\sqrt{13}a_0$ and $3a_0$, respectively); the integrated "excess heat" being down by a factor of $\frac{1}{1000}$ between the $1T$ and $2H$ polytype of $TaSe_2$ [340 (see Ref. 7) cal/mole vs 0.3 (see Ref. 8)]. As for doping, the strongly suppressent action of anion and particularly cation substitutional doping on lock-in may be gleaned from Ref. 9. In the trigonal prismatic systems even anion mixing can completely suppress the lock-in, and the amplitude of the incommensurate CDW (ICDW) is much reduced, so that the density of states at E_F remains high at low temperatures; the superconducting onset temperature T_s benefits as a result.[10] Appropriately, under pressure the lock-in temperature (T_d) for pure $2H$-$TaSe_2$ is depressed as T_s rises (even though for this material the CDW onset temperature T_0 actually increases; initial rates for T_s + 0.013 °K/kbar; T_d − 2.79 °K/kbar; T_0 + 0.35 °K/kbar; T_s, T_d, and T_0 being 0.15, 92, and 122 °K, respectively, in $2H$-$TaSe_2$).[11]

It is not wished, from this gross contrasting of the $1T$ and $2H$ behavior, to imply that either polytypic family is entirely homogeneous. The peculiar behavior of $1T$-TaS_2 is well documented,[1] while in the $2H$ case, $2H$-NbS_2 shows no CDW transitions at all, and $2H$-$NbSe_2$ no lock-in transition. Furthermore, T_0 falls under pressure in $2H$-$NbSe_2$ and $2H$-TaS_2, unlike the above-quoted rise in $2H$-$TaSe_2$. These differences are somewhat surprising, since diffraction data put very little difference between the instability wave vectors within each family [~$0.285\vec{a}_0^*$ both for $1T$-TaS_2 and $1T$-$TaSe_2$ above T_d (Ref. 1); ~$0.325\vec{a}_0^*$ for $2H$-$TaSe_2$ and for $2H$-$NbSe_2$ at T_0 (Ref. 2)].

Under pressure[2] it is observed for $2H$-$NbSe_2$ that λ_{CDW} edges from $3.08a_0$ toward a lock-in at $3a_0$ (as T_0 falls). Even so it continues still to be slightly incommensurate at 20 kbar.[6] We noted above that for the $2H$ materials the empirically determined energy gain following from ultimate lock-in to the lattice is very small. Lock-in, however, does have a relatively strong effect on the elastic properties of $2H$-$TaSe_2$,[12] and also, as is to be expected, upon all properties that are directly affected by the appearance of a superzone, such as optical selection rules[13,14] or de Haas–van Alphen (dHvA) oscillations.[15] The just completed dHvA measurements[15(b)] in $3a_0$ commensurate $2H$-$TaSe_2$ should be contrasted with the earlier results[15(a)] from incommensurate $2H$-$NbSe_2$ on this point.

When sorting out the details of superlattice behavior, the $2H$ situation does in fact become in certain respects more favorable than the $1T$. We

note that the reduced zone is not quite so small, and it is not skewed with respect to the original crystal axes. Moreover, since the Fermi-surface (FS) gapping and atomic displacements are relatively slight, features can be more readily and reliably mapped through into the superzone condition.

II. SOURCE OF THE CDW-PSD IN $2H$-$TaSe_2$

The seat of the effects themselves in the $2H$ materials remains more difficult to identify. In Fig. 37 of Ref. 1b we identified on a sketch of the $2H$ Fermi surface drawn from Mattheiss's augmented-plane-wave results and tight-binding interpolation,[16] the most likely site for $\frac{1}{3}\vec{a}_0^*$ nesting as being across the ML axes, akin to the situation in the $1T$ polytype. However, the surface portrayed there would, we now feel, lead to effects stronger than those actually appearing (even though the two sheets of FS may counteract each other in the selection of an instability wave vector). Recently Wexler and Woolley[17] have produced new band structures for the $2H$ family. While these band structures seem at a glance virtually identical to those of Mattheiss, there are small but significant changes. For example, the $p \rightarrow d$ gap is reduced virtually to zero, in better agreement with photoemission results.[18] A more important change, showing in the Fermi-surface geometry, is that the undulating cylinders up the KH axes are more circular than triangular in shape. This diminishes significantly the degree of Fermi-surface "nesting" under vectors close to $\frac{1}{3}\vec{a}_0^*$.

Ricco *et al.*[19] working with Wexler and Woolley's calculations have very recently made an evaluation of $\chi^0(\vec{q}_{\Gamma M})$ in the single-band approximation and find a broadly humped form. This in fact peaks out at $0.305\vec{a}_0^*$, and not at $0.325\vec{a}_0^*$ (the wave vector with which the CDW actually appears at T_0). It may be that other factors beyond simply the bare susceptibility $[\chi^0(\vec{q})]$ take the peak in $\chi(\vec{q})$ closer to $\frac{1}{3}\vec{a}_0^*$. The important point, as Ricco *et al.* stress, is that given this band structure $\chi^0(\vec{q})$ is very high over a broad range of $\vec{q}$ around $0.3\vec{a}_0^*$, and that significant contributions are still being made to χ^0 over energy increments lying up to ± 0.15 eV from E_F. The reason for this is that the density of states in the vicinity of the Fermi energy is very large. The narrowness of the "d_{z^2}" band ($1\frac{1}{4}$ eV), and the presence of critical points at Γ and M, and a saddle point in ΓK, all within $\frac{1}{4}$ eV of E_F, are compounded to produce a very non-two-dimensional density-of-states profile. The $1T$ case shows, by contrast, the classic flat square-edged profile, and $N(E_F)$ is only ~0.6 states/(eV cation spin) as against ~2.5 in the $2H$ case (for which E_F is so close to the strong peak in the density of states).[16] Myron *et al.*[20] had, prior to Ref. 19, calculated $\chi^0(\vec{q})$ for $1T$-$TaSe_2$, and found there a fairly well-defined maximum at $0.278a_0^*$ ($1/\sqrt{13} = 0.2773$) of magnitude equivalent to 0.62 states/(eV cation spin) $[(\chi_p)_v = 2\mu_B^2 N(E_F)]$. The broad feature now determined in the $2H$ calculation of $\chi^0(q)$,[19] in being equivalent to 2.2 states/(eV atom spin) preserves, it is to be noted, the approximately 4 to 1 ratio in $N(E_F)$ quoted above. The difference, then, between the two cases in their drive toward adoption of a CDW state, is, as might have been suspected, not a question of intensity but of specificity.

Although the calculation of Ref. 19 on $2H$-$NbSe_2$ was not extended all the way back to Γ, it is apparent that $\chi^0(0)$ is going to be $\sim\frac{1}{3}\chi^0_{\max}(q)$. This translates to a value of 100×10^{-6} emu/mole for $\chi^0(0)$ on a free-electron basis. The observed susceptibility of 200×10^{-6} (uncorrected for diamagnetism), indicates that substantial many-body enhancement of $\chi^0(0)$ is active in the $2H$ materials. This is the sort of activity that could convert the peak in $\chi^0(q)$ at $0.305\vec{a}_0^*$ above to one in $\chi(\vec{q})$ at $0.325\vec{a}_0^*$ without calling for further adjustment of the band structure.

If we are now to accept the Wexler and Woolley band structure as it stands, for it apparently is an improvement in the right direction on several points over the earlier augmented-plane-wave calculation, this leads to interesting conclusions concerning just what role the ΓK saddle point might have in promoting the "$\frac{1}{3}\vec{a}_0^*$" instability of the $2H$ materials. Working from Mattheiss's results, Rice and Scott[21] have suggested that this saddle point might in fact occur very close in energy ($\sim kT_0$ or 0.01 eV to the Fermi surface, and at a wave vector close to $\frac{2}{3}\Gamma\vec{K}$. They show that these circumstances can cause a rather narrowly sited CDW-PSD instability for wave vector "$\frac{2}{3}\vec{a}_0^*$," indistinguishable in practice from a "$\frac{1}{3}\vec{a}_0^*$" instability. The new band calculation, however, lends support to neither of the fortuitous contentions required to make the saddle-point mechanism work in these materials, since the saddle point shows up much closer to $\frac{1}{2}\Gamma\vec{K}$ than $\frac{2}{3}$, and it falls ~0.2 eV below E_F. Direct resolution of this matter might be made experimentally if substitutional doping by d^2 MoS_2, etc., could be accomplished without disorder suppressing the CDW. The fuller Fermi sea should cause a "$\frac{1}{3}\vec{a}_0^*$" spanning vector to increase to and beyond $0.333\vec{a}_0^*$, but would negate saddle-point nesting, as E_F is raised further.

Whatever mechanism drives the "$3a_0$" instability, one must concede that it is a strikingly persistent

feature, considering the weakness of its final expression. It survives all symmetry changes wrought in both the electron and phonon dispersion curves under change of polytype, whether that change involve simple c-axis stacking ($3R, 4Hc$), or, more strikingly, a coordination alternation ($4Hb, 6R$).[22] Mattheiss has shown that the general shape of the band dispersion is determined, by and large, within a single sandwich [Ref. 16, Fig. 12(c)], (though this is not so, of course, for the cell-size- and symmetry-dependent multiplicity of bands). More evidence for the rather low specificity of the effect comes from the phonon dispersion curves obtained by neutron diffraction.[2,23] Wakabayashi *et al.*[23] have drawn attention in a comparison of the 300 °K results on d^1 $2H$-$NbSe_2$ with those on d^2 $2H$-MoS_2, to the fact that there is in the d^1 case a general depression in all the acoustic branches from $0.15\vec{a}_0^*$ right on through to the zone boundary at $0.5\vec{a}_0^*$. It is also to be noted that the "$\frac{1}{3}\vec{a}_0^*$" phonon is possibly not driven completely soft before the second-order CDW onset is reached in $2H$-$TaSe_2$ at 122 °K (Ref. 2 and more recent data). Finally we note that the chalcogen deficient $2H$ material is known to favor a $2a_0$ over a $3a_0$ instability [Ref. 1(b), Sec. VII D]. The generally high $\chi^0(q)$ evaluated in Ref. 19 would seem able to embrace all these features.

For the $2H$ Ta materials, CDW onset and lock-in lead to a 10 to 20% decrease in $\chi(0)$. This serves as a rough measure of the proportion of the Fermi surface removed by gapping during these processes. The conductivity surprisingly improves both at onset and lock-in (see Ref. 11). This, as Rice and Scott point out, probably signifies that the high density-of-states scattering sinks in the vicinity of the ΓK saddle points are diminished appreciably in the course of these events. We shall shortly see how interpretation of the recent dHvA results[15(b)] inexorably makes for just such a modification in the Fermi surface.

The Fermi surface for the $2H$ materials consists of empty undulating "cylinders" of approximately equal cross section running up the ΓA and KH axes, there being two of the latter and one of the former type per zone. These cylinders are double walled, apart from where tied by symmetry over the top and bottom faces (ALH) of the conventional single zone. As pointed out by Wexler and Woolley,[17] under space group D_{6h}^4 (as hcp metals) the degeneracy is there of the time reversal type, and the Fermi surface does not come into these faces at right angles, but rather with the two surfaces coming in at equal and opposite angles. Hence each double surface may be folded out into a single continuous surface in a double zone scheme. This point was missed in our drawing of the Fermi surface in Ref. 1(b) [Fig. 27(a)]. It has the important consequence for the present work that the plane ALH does not provide extremal orbits, only the plane ΓMK and its folded-out partner (see Fig. 5).

The results of Wexler and Woolley given in Fig. 6 of Ref. 17, show that for the sulfides the ΓA and KH cylinders undulate in phase up the double zone, whilst for the selenides they are out of phase. This apparently is not significant in the governance of CDW-PSD behavior through the family. The latter seems to be determined in the main by the geometry of the KH cylinders, coupled of course with the elastic properties of the compound concerned. As noted earlier, T_0 falls under a reduction in molecular weight, and the associated rise in phonon energies[2] and elastic constants.[12]

Figure 1 provides an extended view of the projected Fermi surface of $2H$-$TaSe_2$, following the results of Wexler and Woolley (their Fig. 6). In their Fig. 7 they indicate that the most favorable though rather indifferent nesting comes under vectors of the family $\frac{1}{3}\vec{a}_0^*$, for which the inner KH cylinder here now nests (on the ΓMK plane), as well with itself as with its neighbor (a fair contribution also coming from the inner surface around Γ). We illustrate this in detail in Figs. 2 and 3. It is easy to see, by sliding two copies of the Fermi surface over each other, how the calculated high value of $\chi^0(\vec{q})$ is maintained over a wide range of $\vec{q}$, as in rapid succession various features are roughly brought into a nesting relationship. However, none of those circumstances is

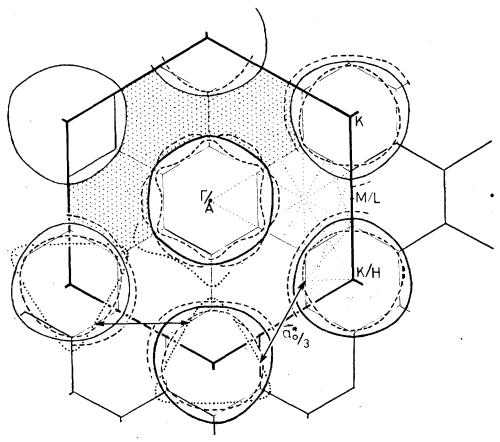

FIG. 1. Projection of Wexler and Woolley's (WW) Fermi surface for $2H$-$TaSe_2$ in comparison to one based on Mattheiss's calculations. Small hexagons are the reduced zone scheme for the $3a_0$ superlattice. Fine dotted lines are appropriate to the superlattice extended zone scheme, see Fig. 4. Heaviest outline is the WW surface on the plane ALH, and is flanked by the dashed outlines of the two sheets on the ΓMK plane. Heavy dotted outline is the Mattheiss ALH result.

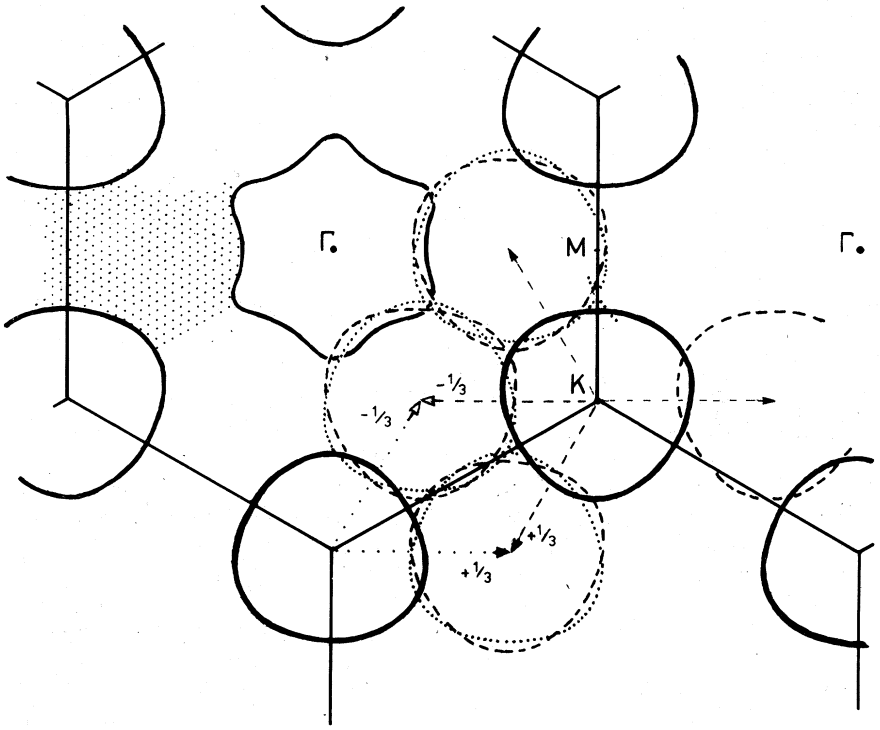

FIG. 2. Inner ΓMK WW Fermi surface, indicating (by the displaced dotted and dashed outlines) the conditions for moderately good nesting under vectors $\pm\frac{1}{3}\vec{a}_0^*$. Other sheets are less conducive, see Fig. 3.

as marked as it was for $\frac{1}{3}\vec{a}_0^*$ when using a Fermi surface of the form used in Fig. 37 of Ref. 1(b). A segment of that surface has been included here in Fig. 1, along with a couple of spanning vectors across the M point. (Note, when the KH cylinders are so triangular, self-nesting under this vector is reduced, compared with the situation in Fig. 2.) We see in Fig. 3 that very significant contributions to $\chi^0(\vec{q})$ are associated with points close to $\frac{2}{3}\Gamma\vec{K}$, where we are just coming out of the saddle-point region around $\frac{1}{2}\Gamma\vec{K}$, and the bands are still relatively flat.

If, as indicated by the experimental change in $\chi(0)$, as much as 10% of the Fermi surface is gapped below T_0, this would be met by about $\frac{1}{6}$ of each KH cylinder, arising in two families each of three segments. Lock-in $3a_0$ augments this fraction somewhat, as we shall see in detail in Sec. IV. Prior to that, let us take note of what happens to the electrical transport properties under the action of the ICDW on the Fermi surface.

III. CHANGE IN TRANSPORT PROPERTIES FROM CDW

The resistivity of $2H$-$TaSe_2$ at 300 °K is rather high, being, at $\sim 1.2\times10^{-4}$ Ω cm, twice that even of the d^1 layer halide (1T) LaI_2.[26] The temperature coefficient of resistivity is nonetheless much as for silver, it being the general level of resistivity which is high. The low-temperature resistivity found[10] in the absence of a CDW in $4Hc$-$TaS_{1.2}Se_{0.8}$ and $2H$-$TaS_2\cdot pyr_{1/2}$ is $\sim 0.5\times10^{-4}$ Ω cm. At 300 °K, the Seebeck coefficient is negative[24] (~ -10 μV/°K) and the Hall coefficient is positive[25] ($\sim +2\times10^{-4}$ cm^3/C). The conflict here in signs indicates a two-carrier-type situation, as also does the magnitude of R_H. The cation and carrier density for $2H$-$TaSe_2(d^1)$ is 1.55×10^{22}/cm^3, having a R_H equivalence of $\sim 4\times10^{-4}$ cm^3/C or twice the measured value.

It is possible from an inspection of Wexler and Woolley's band structure to see how this comes about. The ΓA cylinders we judge to be p-type, particularly the inner one, because of the proximity of the Γ_1^+ critical point to the Fermi level. Although the electrons on the KH cylinders help to outnumber the p-type carriers active on the ΓA cylinder by ~3:1, these n-type carriers are much heavier, since the FS intersects the bands involved close to their points of inflection. Use of

$$R_H=\frac{p-n(\mu_e/\mu_h)^2}{[p+n(\mu_e/\mu_h)]^2}\,;\quad S=\frac{pe\,|S_h|-ne\,|S_e|}{pe+ne}$$

shows $\mu_e=\frac{1}{8}\mu_h$ taken in conjunction with $n=3p$, to yield $R_H=+2\times10^{-4}$ cm/C, the observed value between 300 °K and T_0. The large excess of electrons over holes accounts for the negative Seebeck coefficient.

With the establishment of the CDW, the number of electrons is reduced, and the number of holes rises. The total number of carriers diminishes by ~15% through T_0/T_d. The carrier types now,

we reckon (subsequently see Figs. 8 and 9), are split approximately 0.6 to 0.4, this time in favor of holes (i.e., $p=\frac{3}{2}n$). The Seebeck coefficient does become positive. The new situation necessitates, in order that R_H will match a now negative experimental value of -2×10^{-4} cm^3/C in $2H$-$TaSe_2$ (reached at 40 °K),[25(a)] a reversed mobility ratio of (on the average) $\mu_e\sim 2\mu_h$. As mentioned in Sec. II, after the onset and lock-in of the CDW, ρ diminishes rapidly (approximately as T^2 down to ~20 °K), finally leveling off in the best samples well below 10^{-6} Ω cm.[27] This change in resistivity behavior has been attributed[21] to reduction of the high density-of-states peak close to E_F (that arises in large part from the ΓK saddle point), thereby increasing τ and μ.

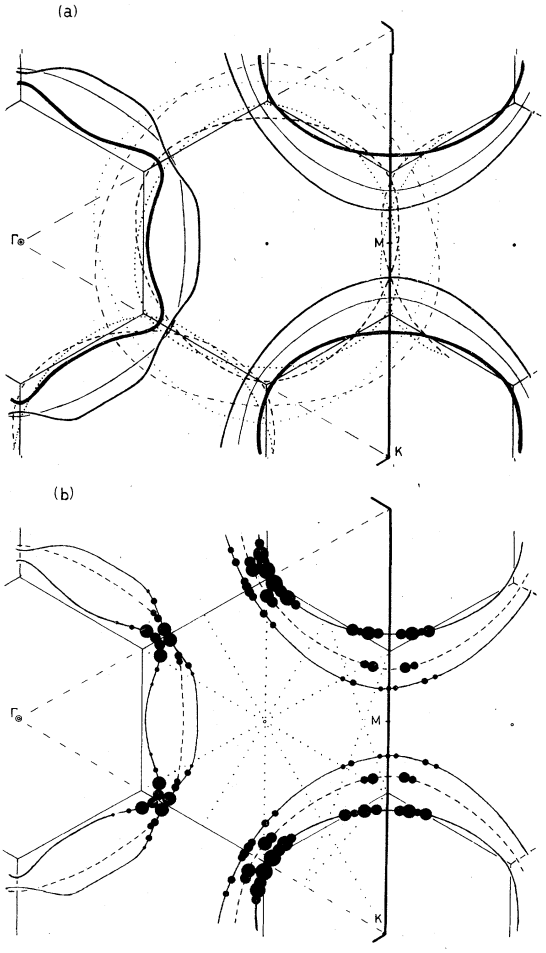

FIG. 3. Combination of an expanded version of Figs. 1 and 2, now displaying both sheets and both planes. (a) Shows some of the displaced outlines relevant to building up χ^0 ($q_0=\frac{1}{3}\vec{a}^*_0$). (b) Indicates where significant contributions to this quantity arise, prior to actual truncation of the FS by the ICDW.

In Sec. IV, involving detailed interpretation of the de Haas–Van Alphen (dHvA) results for the superlattice phase of $2H$-$TaSe_2$, we see how such modifications in transport properties ought indeed to accompany the adduced reconstruction of the Fermi surface.

IV. DESCRIPTION OF THE CHANGE IN FS OF $2H$-$TaSe_2$ IN COMMENSURATE CDW (CCDW) PHASE, FOLLOWING INTERPRETATION OF dHvA DATA

Although it seems not yet to have been picked up in ir work, gapping directly expressive of the ICDW condition may well be no more than ~0.05 eV or 400 cm^{-1} (i.e., $\lesssim 5kT_0$). [The effects around $\frac{1}{4}$ eV first reported on by Barker,[28] and now in Ref. 13b, presumably follow from the appearance of new critical points close to E_F.] Moreover, this is in the vicinity of points on the Fermi surface where the interaction is most intense. All present evidence suggests that the gapping when commensurate is little more developed. Hence we can look to an overall geometry of the (folded-out) Fermi surface that is not wildly changed, even in the prevailing relatively flat-band situation.

In Fig. 4 construction is given, appropriate to the 3×3 superlattice, of the Brillouin planes and "folded-out" zone fragments out to the ninth zone. These fragments taken together must of course just fill the Brillouin zone of the parent undistorted phase. In the lower part of Fig. 4 the fragments are shown grouped in the customery manner, appropriate to a free-electron system with minimum energy at Γ and E increasing approximately radially over k space. However, it is apparent that this grouping is not appropriate to the present parent situation, for which the energy minimum is found in ΓM about $\frac{2}{3}$ of the way to M. Indeed the repeated zone scheme of the superzone, which had been included in Fig. 1, is seen to provide an associative framework better suited to the present band structure. The Fermi sea is contained entirely within those six repeated superzones centered on the points $\frac{2}{3}\vec{\Gamma M}$; that centered on Γ, and the remaining two centered on K are completely empty. Toward the top of Fig. 4 we indicate then a symmetric breakdown of this occupied region to form extended fragments of superzones labeled b–g. Zones f and g (and also the unoccupied zones k and i) are seen to incorporate Brillouin planes that will lead to Bragg reflections and some gapping. These, in general, lie clear of the Fermi surface, but will be of some importance within zone f. These gaps, being determined by the superlattice potential, are only small, unlike those encountered (given the present band structure) if one were to try the customary structuring

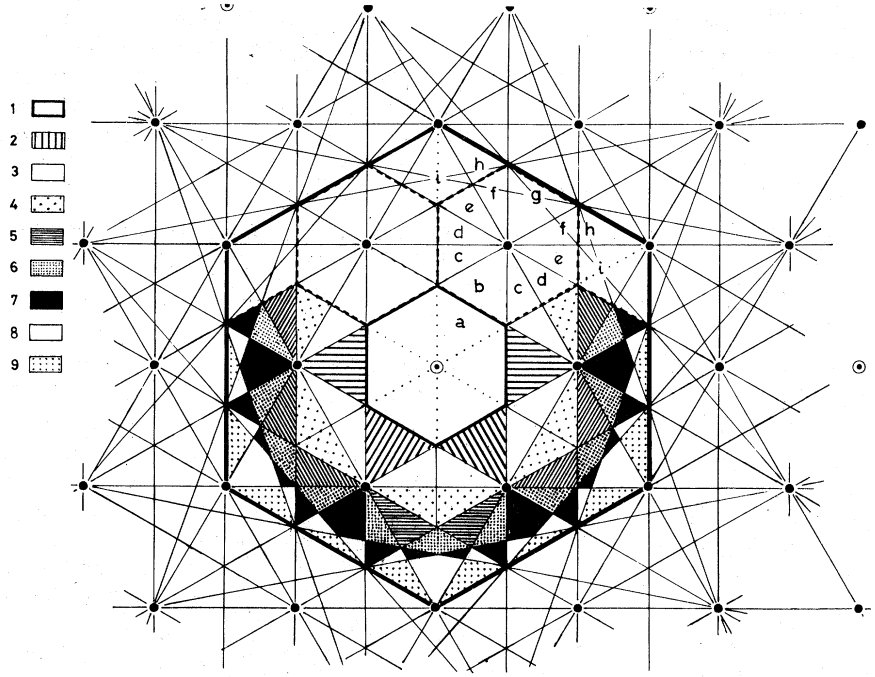

FIG. 4. Extended zone scheme construction for the superlattice $3a_0$ condition. First nine zones just fill the parent Brillouin zone. The $3a_0$ "Brillouin planes" were, for later reference, dotted in already on Figs. 1 and 3(b). Radial grouping of fragments is not the most advantageous in the present case (see text).

of zones 6–9. Zones a–e are seen to refer to the same portions of k space as would zones 1–5, respectively. Planes in k space on which we can expect superlattice gapping in accord with the construction of Fig. 4 have already been incorporated over limited areas of Figs. 1 and 3(b) for later comparison with Figs. 8 and 9.

In assigning the dHvA orbits, we have borne in mind the superlattice enhanced CDW gapping, sited in accord both with the places of superior nesting and with proximity to a saddle point (see Figs. 2 and 3). In any proposed band-folding process one must, of course, appreciate that band hybridization can occur to modify the simple picture. However, since the symmetry remains high in the superlattice condition, many bands are permitted to pass through each other freely. In other cases where band hybridization must occur, it often will fall clear of the Fermi surface. Fortunately in the six zones b–g, the minimum of energy is located near their Γ point. Both calculation[17] and angular photemission[18] have indicated that the minimum energy in the d band falls out not at M, but close indeed to $\frac{2}{3}\Gamma M$ (provider of the Γ point for zones b–g).

Prior to assignment of the dHvA results, the following points should also be made: (a) Time reversal symmetry alone, on the planes ALH of the parent (Fig. 5) or superzones, will not provide the conditions for extremal orbits. (b) dHvA results in $3a_0$ $TaSe_2$ indicate undulating "cylinders" parallel to k_z with only two extremal values each, probably coming again from the two sheets of FS in the $k_z = 0$ plane. (Note for the superlattice we still have the $2H$ condition, i.e., $c = c_0$.) (c) Because of the high hexagonal symmetry remaining in the $3a_0$ phase, the two sheets should stay degenerate (neglecting relativistic effects) at the K points in each reduced zone, as for the parent phase. (d) Despite the mobility in the d band being low relative to a metal like cadmium, magnetic breakdown should be anticipated, even below 50 kG given the present slight gapping of the Fermi surface. (e) Hexagonal rather than trigonal symmetry is preserved in the Fermi surface, through the equivalence of $+q_0$ and $-q_0$ in the CDW-PSD and the fact that $\vec{q}_0$ lies here in the $k_z = 0$ plane, rather than tilted out of it as for $1T$ polytype.[1] (f) Figure 6 makes some representation of what is involved

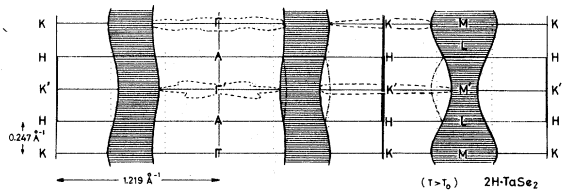

FIG. 5. Vertical section of the WW FS for $2H$-$TaSe_2$, shown in the double zone scheme. Plane ALH does not give extremal orbits. Some indication is given of the extremal orbits in the ΓMK plane, in order to help visualize the types of deviation from a $\sec\theta$ change in area met upon tilting field and orbit normal from k_z. [Note that in Fig. 27 of Ref. 1(b) the vertical scale is a factor of 1.5 too small.]

when an incommensurate CDW becomes commensurate. The extra electrons required in case (b) are drawn from elsewhere in the zone, especially from a region such as that in case (a) just over the superzone boundary.

The dHvA data[15(b)] collected from $2H$-$TaSe_2$ at 1.3 °K ($H \sim 30$–100 kOe) are shown in Fig. 7. By the behavior furnished under progressive tilting of the field from the c axis, it was clear that the data relate to four different types of undulating "cylinder" axes parallel to k_z. As may be appreciated by referring to Fig. 5, the undulations in the fourth and largest cylinder type (represented by orbits ζ and μ) are the most pronounced. All four types however, show, a 25 to 30% variation (up k_z) in their area of cross section (meaning a 15% variation in radius for the equivalent circular orbit). Secant θ plots through the twin-branch intersection points yield for each type an approximate average cylinder size. Unfortunately no information may be gained in the present circumstances concerning the *shape* of the various extremal orbits (ϕ variation). Orbit ζ corresponds to a fairly large area, being just over half the superzone size. For $\vec{H} \| \vec{c}$, orbit η is of almost the same size as the single orbit detected previously[15(a)] in $2H$-$NbSe_2$ (incommensurate, and not so pure), but the tilt characteristics in that case were quite different, appertaining to a very flat ellipsoid of revolution.

The task now presented is to make disposition of the various "cylinders" within the reduced zone. Each type may be sited either singly and centrally, or set in symmetric array about the zone. Appreciable deviations from the circular are quite in order, but there exists, of course, the ultimate constraint that the Fermi surface must en-

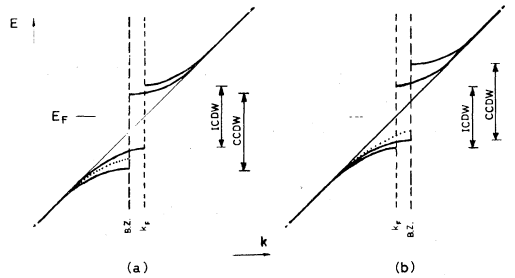

FIG. 6. Illustration of Fermi surface gapping under a CDW, and its modification in the proximity of a superlattice zone boundary for $T < T_d$ (the superlattice lock-in temperature). Dotted curve in the superlattice condition makes a rough apportionment of the total stabilization energy between the modified CDW and its commensuration energy, which can be coming out prior to ultimate lock-in.

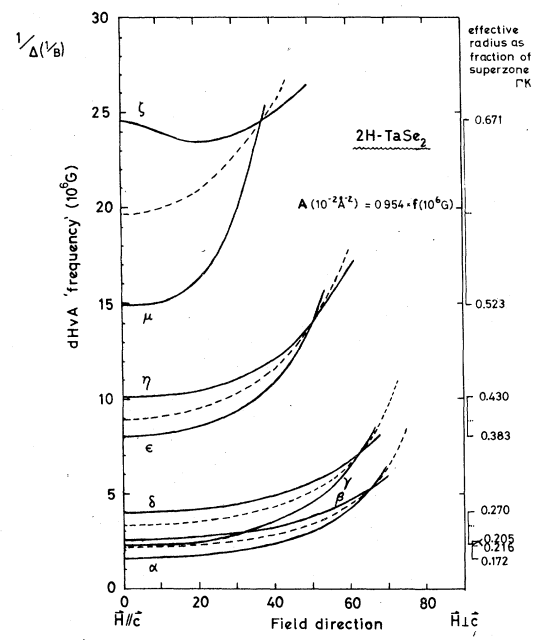

FIG. 7. dHvA results for $3a_0$ $2H$-$TaSe_2$, after Ref. 15(b). Data are appropriate to four types of undulating c-axis cylinders, the orbits lying in planes ΓMK and $\Gamma'M'K'$ of the superlattice FS. Average dashed secθ curves do not necessarily give information about ALH (see Fig. 5). Equivalent circular radii are used in constructing Figs. 8 and 9.

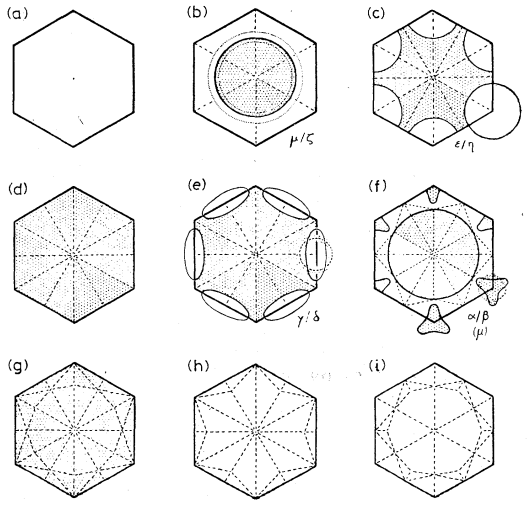

FIG. 8. Completion of the jigsaw of fragmented superzones for the $3a_0$ condition that is most appropriate to the present band structure (see text), together with their filling in the case of $2H$-$TaSe_2$ below T_d. dHvA orbits have been accommodated in the following way: α/β in f, γ/δ in e, ϵ/η in c, μ/ξ in b. Figure 8 should be closely compared with Fig. 9, for illumination of the distortions made in zones e and f from the equivalent circular radii.

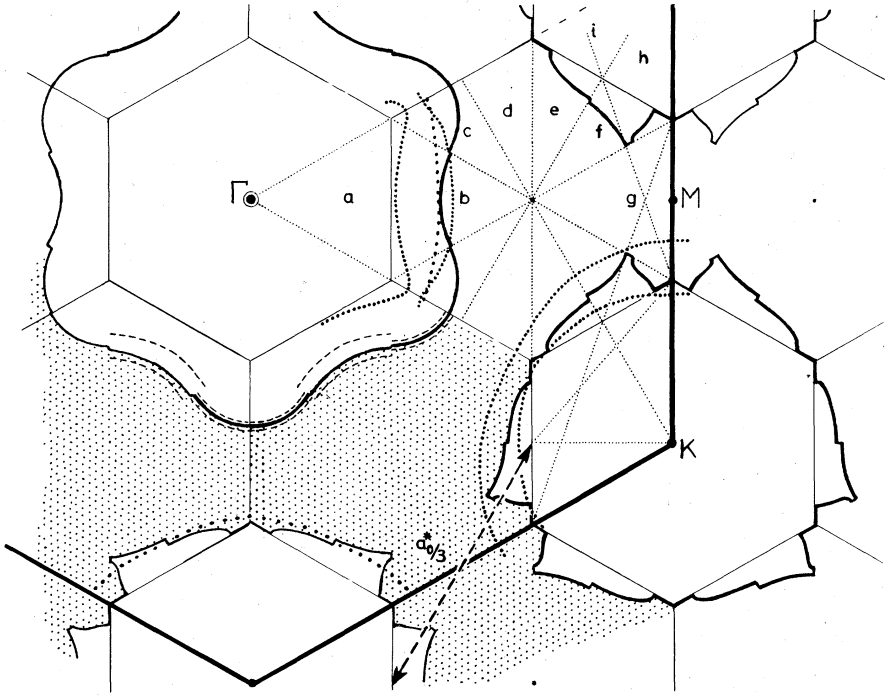

FIG. 9. Reconstructed FS for $2H$-$TaSe_2$ in the CCDW condition (for the plane ΓMK). Small portion of the parent FS is given for comparison (heavy dots). Lightly dotted lines indicate planes over which gapping may arise under a $3a_0$ potential (see Fig. 4). Only for the surface around Γ are the two sheets of FS (appropriate to c_0 equal to double sandwich) shown individually (dashed). About 15% of the surface shown around K is gapped.

close the equivalent of $\frac{9}{2}$ superlattice zones in order to meet the average d^1 condition.

What seems a suitable solution to this problem is developed in Figs. 8 and 9. Cylinder ζ/μ is centrally sited in superzone b. There it forms part of a somewhat expanded surface about the parent ΓA axis. Such is also the case for cylinder ϵ/η, shown centered on the corners of superzone c. Cylinders γ/δ and α/β each form part of the more strongly modified surface around the parent KH axes. γ/δ outlines an ellipse in superzone e around each ML axis, while α/β traces a trefoil around the KH axes in superzone f. Superzone f also contains a central piece of FS of the same size as ζ in superzone b.

With Fig. 10 we display together all the active and often intersecting bits of Fermi surface. These derive from zones b, c, e, f, and g. Depending on what degree of hybridization actually arises around each implied band crossing in the superzone, we may have to invoke magnetic breakdown before the principal orbits collected here do indeed become the observed ones. In practice only orbit ζ, which makes several oblique crossings of ϵ/η, needs high fields for its observation. Graebner did in fact note several small orbits, of area $< \frac{1}{3}\alpha/\beta$ (i.e., < 0.5 MG), which possibly are due to various minor orbits that may be followed on Fig. 10 (especially after the inclusion of hybridization and spin-orbit coupling).

The above scheme can be seen, from inspection of the (c-axis averaged) folded-out version of the Fermi surface given in Fig. 9, to entail the requisite 50% filling of the parent zone. Electrons tend to have been moved outwards away from Γ, in the parent ΓK, saddle-point containing, directions. We saw from Fig. 3 that nesting was most favor-

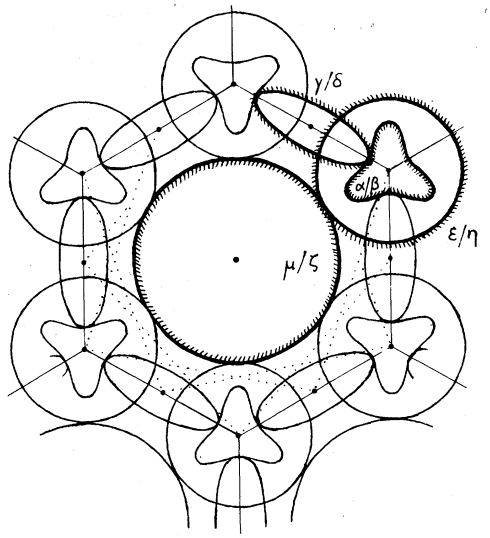

FIG. 10. Various elements of FS have been collected into one reduced superzone. (Hatching is toward the occupied side of the four detected cylinders.) All gapping ensuing from the CCDW state is taken to be sufficiently slight for magnetic breakdown to occur permitting observation of these major orbits. Four cylinders are given their average size. Hence orbit ζ will intersect orbits η.

able in the region around $\frac{2}{3}\Gamma\vec{K}$. In Fig. 9, that gapping we find to have been pulled over to the superzone boundary, after the manner indicated in Fig. 6. Similar behavior occurs at two points in superzone f. We find none of the Fermi surface around ΓA to be removed, apart from the small radial superlattice gaps, but the gapping around KH, as was gathered earlier from the electromagnetic properties, is moderately extensive. The *active* area is cut by as much as $\frac{1}{5}$. Below T_d carriers around the old KH axes will include holes (as in zone e) besides electrons (zone f). The latter are probably the lightest carriers now present, and are certainly much lighter than any of the original carriers. Together with the reduction in scattering, the appearance of such carriers may well account for the much improved conductivity below T_0/T_d. They also drive the Hall coefficient negative.

The above accomodation of the dHvA data does then accord suitably with the conjectured physics of what is going on at the transitions in $2H$-$TaSe_2$. From this point of view the above assignment of the dHvA orbits seems unique. In particular, it is not feasible to commence by fitting out zone b in any other manner. Also the 50% overall filling requirement ($\equiv\frac{9}{2}$ superzones) is very restrictive, yet it is exactly satisfied by the above scheme. Placing cylinder 4 centrally in zone b, moreover, makes sense also in that, with its large disparity in area between orbits ζ and μ, it matches the original tendency of the band structure to produce a rim in toward the Γ_1^+ state (see Fig. 1).

V. FINAL REMARKS

We have seen above how the CDW instability in $2H$-$TaSe_2$ probably arises and proceeds. One might even try to ascribe the observed onset with $q_0 = 0.325a_0^*$, rather than with $0.333a_0^*$ (as used in Figs. Figs. 2 and 3), to a somewhat improved nesting at this wave vector of the (inner) displaced KH cylinder with its KH neighbor and with the zone center cylinder, at the expense of self-nesting. This could be what the shifted peak in the calculation of Ref. 19 expresses. Unfortunately, the same calculation has not been made for the other members of the $2H$ family. However, from inspection of Wexler and Woolley's band structures and Fermi surfaces, for each of the four compounds $TaSe_2$, TaS_2, $NbSe_2$, NbS_2,[17] it is not evident why the path of decreasing activity is going to follow this, the experimental order. In being the order of falling molecular weight it is, of course, simultaneously the order of falling spin-orbit splitting, a factor currently absent from the calculations. Such splitting extending out from K_5 into ΓK might be of importance here.

The above order is in addition, naturally, the order of rising phonon frequencies, and it is quite probable that a more profitable line of action at this point would be to investigate the electron-phonon interaction as a function of q. Such a study should also be of value in understanding the variation of T_s (superconducting onset) through the family, including its change under pressure.[29] The same goes for the changes in T_0 and T_d under pressure.[8,11,12] Comparative measurements to low temperatures of S, R_H, and ρ on good-quality speciments of all four compounds are also now worth pursuing. These data would help better to establish the changing character of the Fermi surface, and its degree of responsibility for the evolution of CDW-PSD behavior through the family. The crystals of $2H$-TaS_2 and $2H$-NbS_2 currently available do not permit dHvA work.

ACKNOWLEDGMENTS

The author would like to thank J. Graebner and L. F. Mattheiss for several discussions concerning this work.

[1](a) J. A. Wilson, F. J. Di Salvo, and S. Mahajan, Phys. Rev. Lett. 32, 882 (1974; (b) Adv. Phys. 24, 117 (1975).
[2](a) D. E. Moncton, J. D. Axe, and F. J. Di Salvo, Phys. Rev. Lett. 34, 734 (1975); (b) D. E. Moncton, Ph.D. thesis (M.I.T., 1975) (unpublished).
[3]R. Brouwers and F. Jellinek (unpublished) (see Bari Conference, abstracts, p. 63, Sept. 1976).
[4](a) G. K. Wertheim, F. J. Di Salvo, and S. Chiang, Phys. Lett. A 54, 304 (1975); (b) Phys. Rev. B 13, 5476 (1976).
[5]M. Eibschutz and F. J. Di Salvo, Phys. Rev. Lett. 36, 104 (1976).
[6]C. Berthier, D. Jerome, P. Molinie, and J. Rouxel, Solid State Commun. 19, 131 (1976).
[7]F. J. Di Salvo, R. G. Maines, J. V. Waszczak, and R. E. Schwall, Solid State Commun. 14, 497 (1974).
[8]M. Barmatz, L. R. Testardi, F. J. Di Salvo, and J. M. E. Harper, Phys. Rev. B 13, 4637 (1976).
[9]F. J. Di Salvo, J. A. Wilson, B. G. Bagley, and J. V. Waszczak, Phys. Rev. B 12, 2220 (1975).
[10]J. F. Revelli and W. A. Phillips, J. Solid State Chem. 9, 1976 (1974); J. F. Revelli, Ph.D. thesis (Stanford University, 1973) (unpublished).
[11]C. W. Chu, L. R. Testardi, F. J. Di Salvo, and D. E. Moncton, Phys. Rev. B 14, 464 (1976).
[12]M. Barmatz, L. R. Testardi, and F. J. De Salvo,

Phys. Rev. B 12, 4367 (1975).
[13](a) J. C. Tsang and M. W. Shafer, Solid State Commun. 19, 611 (1976); (b) G. Campagnoli, A. Gustinetti, A. Stella, and E. Tosatti (unpublished) (see Bari Conference on Layered Compounds, Abstracts, p. 63, Sept. 1976).
[14](a) J. E. Smith, J. C. Tsang, and M. W. Shafer, Solid State Commun. 19, 283 (1976); (b) E. F. Steigmeier, G. Harbeke, H. Auderset, and F. J. Di Salvo, Solid State Commun. 20, 667 (1976).
[15](a) J. E. Graebner and M. Robbins, Phys. Rev. Lett. 36, 422 (1976); (b) J. E. Graebner, Solid State Commun. 21, 353 (1977).
[16]L. F. Mattheiss, Phys. Rev. B 8, 3719 (1973).
[17]G. Wexler and A. M. Woolley, J. Phys. C 9, 1185 (1976).
[18]N. V. Smith and M. M. Traum, Phys. Rev. B 11, 2087 (1975) (see Figs. 11 and 12) and (private communication).
[19]B. Ricco, V. Heine, M. Schrieber, D. Titterington, and G. Wexler (unpublished),
[20]H. W. Myron, J. Rath, and A. J. Freeman (unpublished); A. J. Freeman, H. W. Myron, J. Rath, and R. P. Gupta, Int. J. Quant. Chem. Suppl. 9, 535 (1975).
[21]T. M. Rice and G. K. Scott, Phys. Rev. Lett. 35, 120 (1975).
[22]F. J. Di Salvo, D. E. Moncton, J. A. Wilson, and S. Mahajan, Phys. Rev. B 14, 1543 (1976).
[23]N. Wakabayashi, H. G. Smith, and H. R. Shanks, Phys. Lett. A 50, 367 (1974).
[24](a) T. H. Geballe, AIP Conf. Proc. 4, 237 (1972); (b) D. J. Huntley and R. F. Frindt, J. Can. Phys. 52, 861 (1972).
[25](a) N. H. S. Lee, M. Garcia, H. McKinzie, and A. Wold, J. Solid State Chem. 1, 190 (1970); (b) D. J. Huntley and R. F. Frindt, J. Can. Phys. 52, 861 (1972).
[26]J. D. Corbett, R. A. Sallach, and D. A. Lokken, Adv. Chem. 71, 56 (1967).
[27]F. J. Di Salvo and J. V. Waszczak, J. Phys. (Paris) (Colloq.) 37, C4-157 (1976).
[28]A. S. Barker, J. A. Ditzenberger, and F. J. Di Salvo, Phys. Rev. B 12, 2049 (1975).
[29](a) P. Molinie, D. Jerome, and A. J. Grant, Philos. Mag. 30, 1091 (1974); (b) K. Yamaya, J. Phys. Soc. Jpn. 37, 36 (1974); (c) T. Sambongi, J. Low Temp. Phys. 18, 139 (1975); (d) T. F. Smith, R. N. Shelton, and R. E. Schwall, J. Phys. F 5, 1713 (1975).